

UC Berkeley

UC Berkeley Previously Published Works

Title

Engineering Isoprene Synthase Expression and Activity in Cyanobacteria

Permalink

<https://escholarship.org/uc/item/75p0n6sm>

Journal

ACS Synthetic Biology, 6(12)

ISSN

2161-5063

Authors

Chaves, Julie E
Rueda-Romero, Paloma
Kirst, Henning
[et al.](#)

Publication Date


2017-12-15

DOI


10.1021/acssynbio.7b00214

Peer reviewed

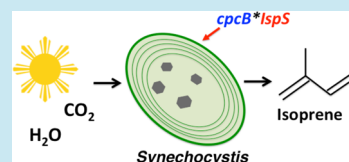
Engineering Isoprene Synthase Expression and Activity in Cyanobacteria

Julie E. Chaves, Paloma Rueda-Romero, Henning Kirst, and Anastasios Melis*

Plant and Microbial Biology, University of California, Berkeley, California 94720-3102, United States

 Supporting Information

ABSTRACT: Efforts to heterologously produce quantities of isoprene hydrocarbons (C_5H_8) renewably from CO_2 and H_2O through the photosynthesis of cyanobacteria face barriers, including low levels of recombinant enzyme accumulation compounded by their slow innate catalytic activity. The present work sought to alleviate the “expression level” barrier upon placing the isoprene synthase (IspS) enzyme in different fusion configurations with the *cpcB* protein, the highly expressed β -subunit of phycocyanin. Different *cpcB**IspS fusion constructs were made, distinguished by the absence or presence of linker amino acids between the two proteins. Composition of linker amino acids was variable with lengths of 7, 10, 16, and 65 amino acids designed to test for optimal activity of the IspS through spatial positioning between the *cpcB* and IspS. Results showed that fusion constructs with the highly expressed *cpcB* gene, as the leader sequence, improved transgene expression in the range of 61 to 275-fold over what was measured with the unfused IspS control. However, the specific activity of the IspS enzyme was attenuated in all fusion transformants, possibly because of allosteric effects exerted by the leader *cpcB* fusion protein. This inhibition varied depending on the nature of the linker amino acids between the *cpcB* and IspS proteins. In terms of isoprene production, the results further showed a trade-off between specific activity and transgenic enzyme accumulation. For example, the *cpcB**L7*IspS strain showed only about 10% the isoprene synthase specific-activity of the unfused *cpcB*-IspS control, but it accumulated 254-fold more IspS enzyme. The latter more than countered the slower specific activity and made the *cpcB**L7*IspS transformant the best isoprene producing strain in this work. Isoprene to biomass yield ratios improved from 0.2 mg g^{-1} in the unfused *cpcB*-IspS control to 5.4 mg g^{-1} in the *cpcB**L7*IspS strain, a 27-fold improvement.



KEYWORDS: carbon partitioning, *cpc* operon, fusion protein, isoprene biosynthesis, isoprene synthase, metabolic engineering, *Synechocystis*, synthetic biology

Engineering of microbes for isoprene (C_5H_8) production has shown a requirement for improvements and modifications to address a number of different rate and yield limitations in the targeted biosynthetic pathway. In general, transgene expression for heterologous product synthesis requires finding and optimizing novel transcriptional regulators such as strong and/or inducible promoters, and ribosome binding sites.^{1–4} Overexpression of terpene synthase enzymes, all of which appear to have a slow k_{cat} , poses an additional unique set of problems. Previous studies, including papers from this lab,^{5–11} focused on isoprene synthase transgene codon-use optimization, mode of cyanobacterial transformation, as well as enhancements in the flux of endogenous cellular carbon to the universal terpenoid precursors isopentenyl-diphosphate (IPP) and dimethylallyl-diphosphate (DMAPP). However, the critical question of the level of expression of the terpenoid biosynthetic pathway transgenes has not been investigated. This question is central to the quest for high yields of isoprene production, measured as the isoprene to biomass carbon partitioning ratio of the process¹² because the terpenoid biosynthetic pathway enzymes, and especially that of the isoprene synthase, have a very slow k_{cat} in the range of $4–5 \text{ s}^{-1}$.^{13,14} A successful strategy by which to overcome the slow k_{cat} of transgenic or native enzymes is to overexpress the enzyme in question so that greater amounts of the desired enzyme could compensate for

their slow k_{cat} . Example of this successful strategy is offered by the ribulose-1,5-bisphosphate carboxylase/oxygenase (Rubisco), which has a slow k_{cat} in the range of $3–4 \text{ s}^{-1}$.¹⁵ Nature’s solution to the slow Rubisco k_{cat} was to substantially enhance the amount of the Rubisco protein in the stroma of the photosynthetic apparatus, making Rubisco one of the most abundant proteins on Earth.¹⁶

This work sought to apply the fusion protein approach and to develop an understanding of the role of recombinant isoprene synthase enzyme concentration and specific activity on the rate and yield of heterologous isoprene production in cyanobacteria. The terpene synthase protein fusion approach^{17,18} was adapted and applied to achieve substantial levels of isoprene synthase expression and recombinant protein accumulation in cyanobacteria. The approach relies on fusing the 5’ end of the terpene synthase gene to the 3’ end of a gene that encodes a highly expressed native protein in the cyanobacterial cell. In this case, the leader gene sequence was the *cpcB* gene encoding the β -subunit of phycocyanin.¹⁹ The β -subunit of phycocyanin is a component of the peripheral rods in the cyanobacterial phycobilisome light-harvesting antenna and is often the most abundant protein in the cyanobacterial

Received: June 16, 2017

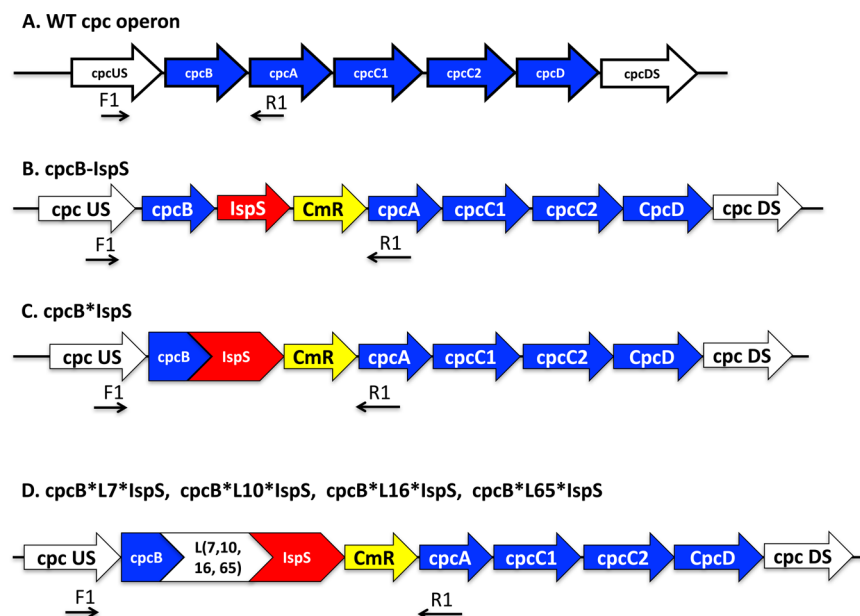


Figure 1. DNA constructs for *Synechocystis* transformant strains were designed to replace the native *cpcB* gene with different versions of the *cpcB* fused to the *IspS* followed by a chloramphenicol resistance (*CmR*) cassette. (A) Schematic of the *cpc* operon in the wild type. (B) In the control *cpcB-IspS* strain, the *IspS* and *CmR* genes were inserted between the *cpcB* and the *cpcA* in a nonfusion configuration. (C) A direct *cpcB*IspS* fusion without a linker, and (D) four different linker-separated versions *cpcB*L7*IspS*, *cpcB*L10*IspS*, *cpcB*L16*IspS*, and *cpcB*L65*IspS* consisting of variable number (7, 10, 16, 65) and composition of amino acid.

cell. This construct resulted in a true overexpression of the *cpcB*IspS* fusion protein, in amounts up to 300-fold greater than what was measured for the heterologous *IspS* gene expression in the absence of a highly expressed leader fusion protein. However, direct fusion of the *IspS* to the *cpcB* gene resulted in very low isoprene synthase specific-activity. To alleviate possible masking or allosteric effects of the *cpcB* protein on the catalytic site of the *IspS*, and hopefully alter the folding pattern of the fusion protein, linker constructs were designed²⁰ and applied between the *cpcB* leader and *IspS* fusion proteins. The use of linker amino acids between the *cpcB* and *IspS* proteins had a significant positive effect on isoprene synthase enzymatic activity, suggesting feasibility of engineering the isoprene synthase activity by regulating distance and folding pattern between the two proteins and thereby improving reactant access to the catalytic site of the terpene synthase.

RESULTS

***Synechocystis* Transformations.** The *cpcB-IspS*, *cpcB*IspS* and *cpcB*L(7,10,16,65)*IspS* constructs (Figure 1) were introduced into the *Synechocystis* genomic DNA at the *cpc* locus via double homologous recombination. Each of the *cpcB*IspS* and *cpcB*L(7,10,16,65)*IspS* fusion constructs with the attendant chloramphenicol resistance cassette (*CmR*) replaced the native *cpcB* gene, while maintaining the rest of the native *cpc* operon (*cpcA*, *cpcC1*, *cpcC2*, *cpcD*) in place (Figure 1). In the control strain (Figure 1, *cpcB-IspS*), the *IspS* gene and its corresponding *CmR* cassette were inserted in-between the *cpcB* and *cpcA* genes without a fusion between any of these genes/proteins. A more detailed schematic presentation of the linker amino acids used between the *cpcB* and *IspS* fusion constructs is shown in Figure 2. Detailed nucleotide sequences of the inserted genes are given in the Supporting Information section.

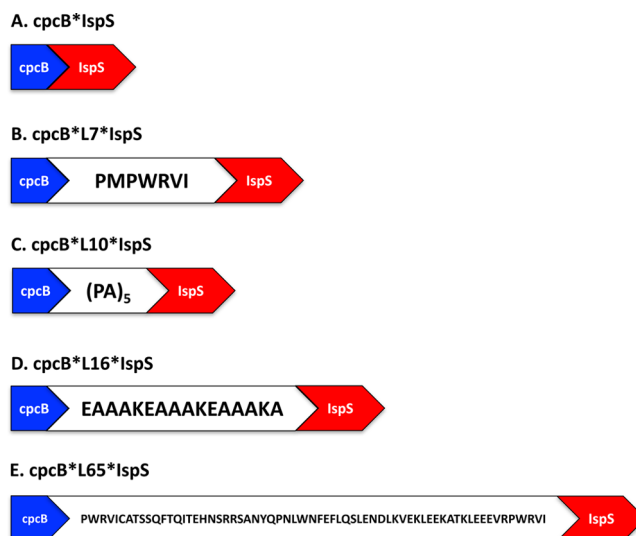


Figure 2. Amino acid sequences of the linkers for each of the fusion strains employed in this work: (A) *cpcB*IspS*, (B) *cpcB*L7*IspS*, (C) *cpcB*L10*IspS*, (D) *cpcB*L16*IspS*, and (E) *cpcB*L65*IspS*.

The state of transgenic DNA copy homoplasmy of the transformant strains was tested by PCR analysis of the *Synechocystis* genomic DNA using primers (forward, F1 and reverse R1, Figure 1) flanking the site of the homologous recombination. These are expected to generate different size products in various transformant DNA, compared to the wild type DNA. In the wild type, the F1 and R1 primers amplified a 1.2 kb product. The *cpcB-IspS* and *cpcB*IspS* strains amplified a 3.8 kb product and failed to amplify the 1.2 kb wild type product (Figure 3A, left-half). Exclusion PCR was performed using the same primers (F1 and R1) with a shorter extension time (30 s), sufficient for the wild type to generate product. The premise of exclusion PCR is that a short extension time

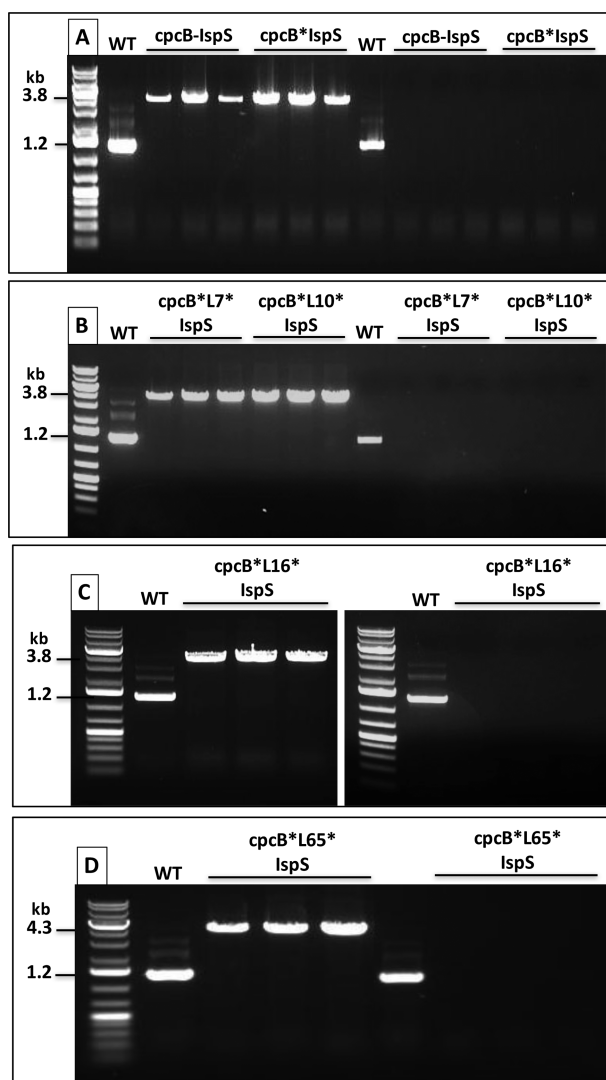


Figure 3. Genomic DNA PCR analysis of wild type and *IspS* transformants. The state of homoplasmy of the transformant strains was tested by PCR analysis of the *Synechocystis* genomic DNA using primers (forward, F1 and reverse, R1) flanking the site of the homologous recombination. In the wild type, the F1 and R1 primers amplified a 1.2 kb product (A–D, left side). The *cpcB-IspS* and *cpcB*IspS* transformants (A), and *cpcB*L(7,10,16)IspS* transformants (B and C), amplified a 3.8 kb product. The *cpcB*L65*IspS* transformant generated a 4.3 kb product (D). Exclusion PCR was performed using the same primers (F1 and R1) with a shorter extension time (30 s), sufficient for the wild type to generate a product, but not so for the transgenes. In each case the wild type generated a 1.2 kb product, while the transgenic strains failed to amplify any product (A–D, right side).

enables product accumulation from short DNA sequences, while excluding those from long DNA sequences under the same conditions and primers. In this case, the wild type amplified the 1.2 kb product (Figure 3A, right-half), while the *cpcB-IspS* and *cpcB*IspS* strains failed to amplify a product. Taken together, these results showed absence of wild type copies of the *Synechocystis* DNA in the *cpcB-IspS* and *cpcB*IspS* transformants, evidence of having achieved transgenic DNA homoplasmy. A similar comparative *Synechocystis* genomic DNA PCR analysis was conducted for the *cpcB*L7*IspS* and *cpcB*L10*IspS* (Figure 3B), *cpcB*L16*IspS* (Figure 3C), and *cpcB*L65*IspS* transformants (Figure 3D). In all cases, the

evidence showed that *Synechocystis* transformants have reached a state of transgenic genomic DNA homoplasmy.

Protein Expression in Wild Type and *IspS* Strains.

Transgenic protein expression levels were determined by SDS-PAGE analysis, loading $\sim 1 \mu\text{g}$ Chl per sample. The wild type recipient strain (Figure 4, WT) showed a dominant protein

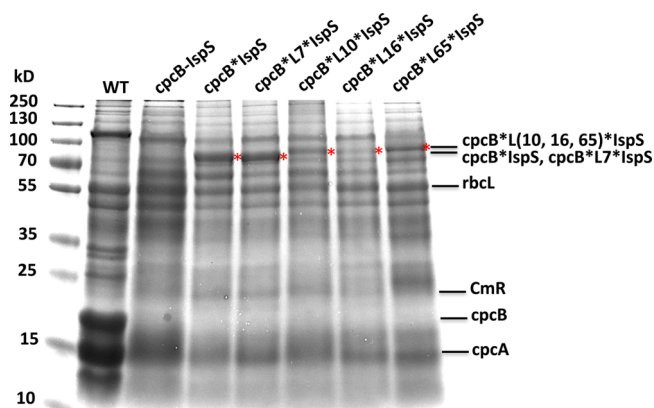


Figure 4. SDS-PAGE analysis of total protein extract from *Synechocystis* wild type and *IspS* transformants. Transgenic protein expression levels were determined from the Coomassie stain of the SDS-PAGE resolved proteins. Lane loadings were $1 \mu\text{g}$ Chl per sample. The wild type strain showed a dominant protein band at about 58 kDa attributed to the large subunit of Rubisco, and abundant protein bands at about 20 kDa from the *cpcB* phycocyanin β -subunit, as well as at about 15 kDa from the *cpcA* phycocyanin α -subunit. The *cpcB-IspS*, *cpcB*IspS*, and *cpcB*L(7,10,16,65)*IspS* transformants all failed to accumulate the 20 and 15 kDa phycocyanin subunits. The *cpcB*IspS* and *cpcB*L(7,10,16,65)*IspS* transformants showed substantial accumulation of the fusion proteins, migrating to about 80–85 kDa (marked by asterisk). A faint band at ~ 24 kDa in this SDS-PAGE analysis was attributed to expression of the chloramphenicol resistance protein.

band at about 58 kDa attributed to the large subunit of Rubisco, and abundant protein bands at about 20 kDa from the *cpcB* phycocyanin β -subunit, as well as at about 15 kDa from the *cpcA* phycocyanin α -subunit. The *cpcB-IspS*, *cpcB*IspS*, and *cpcB*L(7,10,16,65)*IspS* transformants failed to accumulate the 20 and 15 kDa phycocyanin subunits, evidenced by the lack of these proteins from the respective SDS-PAGE lanes (Figure 4). Instead, the fusion *cpcB*IspS* and *cpcB*L(7,10,16,65)*IspS* transformants showed noticeable accumulation of the corresponding fusion proteins, migrating to about 80–85 kDa (Figure 4, protein bands marked by asterisk). Of the various transformants, the *cpcB*IspS*, *cpcB*L7*IspS*, and *cpcB*L65*IspS* constructs showed the highest recombinant protein expression. Constructs *cpcB*L10*IspS* and *cpcB*L16*IspS*, also showed expression of the recombinant proteins, albeit at somewhat lower levels than the *cpcB*IspS* and *cpcB*L7*IspS* fusions. A faint band at ~ 24 kDa in this SDS-PAGE analysis was attributed to expression of the chloramphenicol resistance protein (Figure 4, CmR).

The relative expression of the *IspS* and *cpcB*IspS* fusion proteins was further investigated by Western blot analysis, measuring the specific cross reactions at 65 kDa, attributed to the *IspS* protein, and ~ 80 –85 kDa, attributed to the fusion proteins (Figure 5). In this analysis, cellular extracts were loaded differently than in the SDS-PAGE analysis of Figure 4.

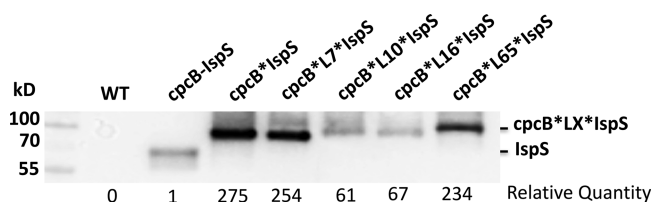


Figure 5. Western blot analysis of wild type and *IspS* transformants using specific polyclonal antibodies raised against the *IspS* protein. Total cell protein extracts were loaded differentially due to great differences in the *IspS* expression level between the nonfused, and fused versions of the constructs. The *cpcB-IspS* sample was loaded with 1 μg Chl, and the *cpcB*L(7,10,16,65)*IspS* samples were loaded with 0.01 μg Chl. The Bio-Rad ChemiDoc imaging system was used to document the Western blot and the Bio-Rad Image Lab software was employed to quantify the relative *IspS* protein levels between the different strains based on the band intensity in the PVDF membrane. “Relative Quantity” of the *IspS* proteins shown here have been corrected for the uneven sample loading.

The WT and *cpcB-IspS* lanes were loaded with 1 μg Chl of cell extract, while the *cpcB*IspS* and *cpcB*L(7,10,16,65)*IspS* sample extracts were loaded with 0.01 μg Chl. This loading adjustment was necessitated because of the asymmetry in the cross-reaction response between the two groups of samples. Results from the intensity of the cross reactions in Figure 5 were consistent with the differential intensity of the Coomassie stain in Figure 4 for the fusion proteins. The *cpcB*IspS*, *cpcB*L7*IspS*, and *cpcB*L65*IspS* proteins were more abundant in the transformant cells than the *cpcB-IspS*, *cpcB*L10*IspS* and *cpcB*L16*IspS* fusion proteins. The Bio-Rad ChemiDoc imaging system was used to document the Western blots and the Bio-Rad Image Lab software was employed to quantify the relative *IspS* protein levels in the different strains. The results were normalized to the cross-reaction intensity of the *cpcB-IspS* sample (=1 relative unit) and corrected for the uneven loading of the *cpcB*IspS* and *cpcB*L(7,10,16,65)*IspS* samples. This semiquantitative Western blot analysis showed the presence of 275, 254, and 234 relative units (Relative Quantity in Figure 5) of *IspS* in the *cpcB*IspS*, *cpcB*L7*IspS* and *cpcB*L65*IspS*, respectively. A lower amount equal to 61 and 67 relative units of *IspS* was measured in the *cpcB*L10*IspS* and *cpcB*L16*IspS* transformants, respectively.

Pigment Analysis. The visual phenotype of the *cpcB-IspS*, *cpcB*IspS* and *cpcB*L(7,10,16,65)*IspS* transformant strains was noticeably different from the wild type and from a strain with a complete *cpc* operon deletion (Δcpc). Absorbance spectra and carotenoid to chlorophyll *a*-ratios were measured to better determine differences in pigment accumulation. The absorbance spectra of wild type cell lysates showed the specific chlorophyll *a* absorbance at 680 and 435 nm, phycocyanin at 625 nm, and carotenoids at 470 nm regions (Figure 6, black line). Carotenoid to chlorophyll (Car/Chl) ratio in the wild type was 0.51:1 (Table 1). The Δcpc strain showed the same chlorophyll *a*-peaks at 680 and 435 nm, but significantly lower absorbance at 625 nm, attributed to the deletion of the *cpc* operon and the ensuing absence of phycocyanin, and retention of allophycocyanin as the only remaining phycobilisome pigment.¹⁹ Carotenoids were slightly elevated in the Δcpc strain (Car/Chl = 0.61:1) compared to the wild type, evidenced both in the absorbance spectra (Figure 6, green line) and from the biochemical analysis in methanol pigment extracts (Table 1), consistent with previous measurements conducted on these

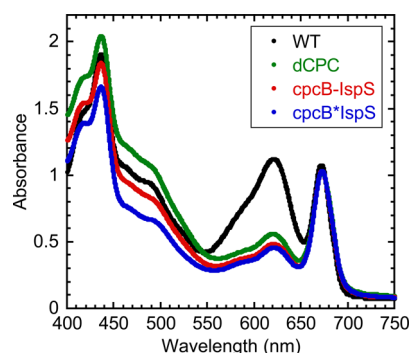


Figure 6. Absorbance spectra of cell lysates were analyzed to determine pigment differentiation in the various fusion strains. The absorbance spectra of wild type cell lysates showed the specific chlorophyll *a* absorbance at 680 and 435 nm, phycocyanin at 625 nm, and carotenoids at about 470 nm regions (black line). The Δcpc strain showed the same chlorophyll *a*-peaks at 680 and 435 nm, but significantly lower absorbance at 625 nm, attributed to the deletion of the *cpc* operon and the ensuing absence of phycocyanin, and retention of allophycocyanin as the only remaining phycobilisome pigment (green line). Carotenoids were slightly elevated in the Δcpc strain relative to the wild type (470 nm region). In the *cpcB-IspS* (red line), *cpcB*IspS* and *cpcB*L(7,10,16,65)*IspS* strains (blue line), the absorbance maximum at 625 nm was also suppressed and at about the same amplitude as that of the Δcpc strain, attributed to inability of these strains to assemble a functional phycocyanin antenna due to fusion of the *IspS* gene to the C-terminus of the *cpcB* gene in the *cpc* operon. Carotenoids (absorbance in the 470 nm region) were slightly lower in these strains relative to that in the wild type.

Table 1. Pigment Analysis Was Conducted on Cells Grown for 96 h in Gaseous–Aqueous Two-Phase Photobioreactors Loaded with 500 mL of 100% CO₂ To Fill the Headspace^a

strain	Car/Chl
Wild Type (WT)	0.51 ± 0.0034
Δcpc	0.61 ± 0.0057
<i>cpcB-IspS</i>	0.42 ± 0.0002
<i>cpcB*IspS</i>	0.36 ± 0.0418

^aContinuous illumination of 100 $\mu\text{mol photons m}^{-2} \text{s}^{-1}$ and temperature of 25 °C were applied during cultivation. Carotenoid and chlorophyll *a* content was measured spectrophotometrically from the absorbance of methanol extracts of the pigment at 470 and 665 nm.

strains.¹⁹ In the *cpcB-IspS*, *cpcB*IspS* and *cpcB*L(7,10,16,65)*IspS* strains, the absorbance maximum at 625 nm was also suppressed and at about the same amplitude as that of the Δcpc strain, attributed to inability of these strains to assemble a functional phycocyanin antenna due to fusion of the *IspS* gene to the C-terminus of the *cpcB* gene in the *cpc* operon. The total carotenoid absorbance was significantly lower in the *cpcB-IspS* (Car/Chl = 0.42:1), *cpcB*IspS* and *cpcB*L(7,10,16,65)*IspS* transformant strains (Car/Chl = 0.36:1) compared to the wild type and Δcpc strains, evidenced both in the absorbance spectra (Figure 6), and from readings of the carotenoid/chlorophyll *a*-ratio in methanol pigment extracts of these strains (Table 1).

The differential pigmentation of the strains examined in this work was reflected in the coloration of the liquid cultures. The wild type appeared blue-green (Figure 7, WT), whereas the Δcpc strain had a more yellowish coloration (Figure 7, Δcpc). The *CpcB* fusion strains had an intermediate greenish

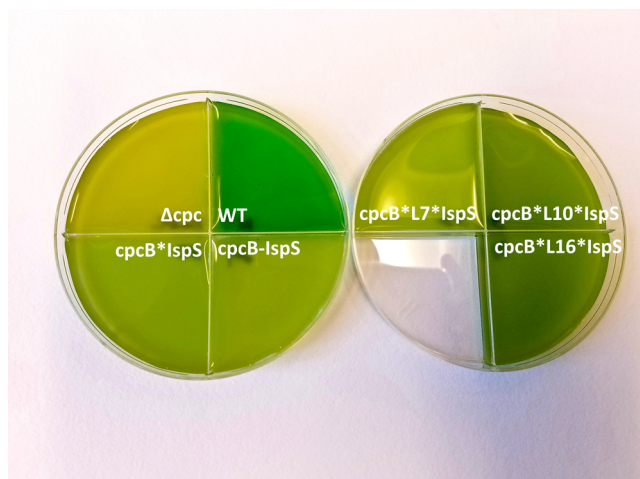


Figure 7. Coloration of cells from liquid cultures of wild type (WT: blue-green), Δcpc (yellow-green), and $cpcB-IspS$, $cpcB*IspS$ and $cpcB*L(7,10,16,65)*IspS$ strains (greenish).

coloration (Figure 7, $cpcB*IspS$ and $cpcB*L(1,10,16)*IspS$). These differences in coloration among the strains were also evident under higher density cultivation conditions (Supporting Information, Figure S10).

Photosynthetic Activity. The functionality of the photosynthetic apparatus, as a result of the disruption of the phycocyanin expression and the introduction of transgenes was measured from the light saturation curves of photosynthesis. The rate of oxygen evolution was negative at zero light intensity and was determined to be in the range of 4 ± 1 mmol O_2 consumption mol^{-1} Chl s^{-1} in the $cpcB-IspS$, $cpcB*IspS$ and $cpcB*L(7,10,16)*IspS$ strains. Increase in the rate of oxygen evolution as a function of light intensity was steeper for the wild type than for the transformants (Figure 8), resulting in dissimilar saturation intensities for the two groups. The light intensity for the saturation of photosynthesis was determined from the intersect of the initial linear increase in the rate of photosynthesis with the asymptotic light-saturated state–state rate (P_{max}). This analysis showed that photosynthesis in the wild type was saturated at about $100 \mu mol$ photons $m^{-2} s^{-1}$,

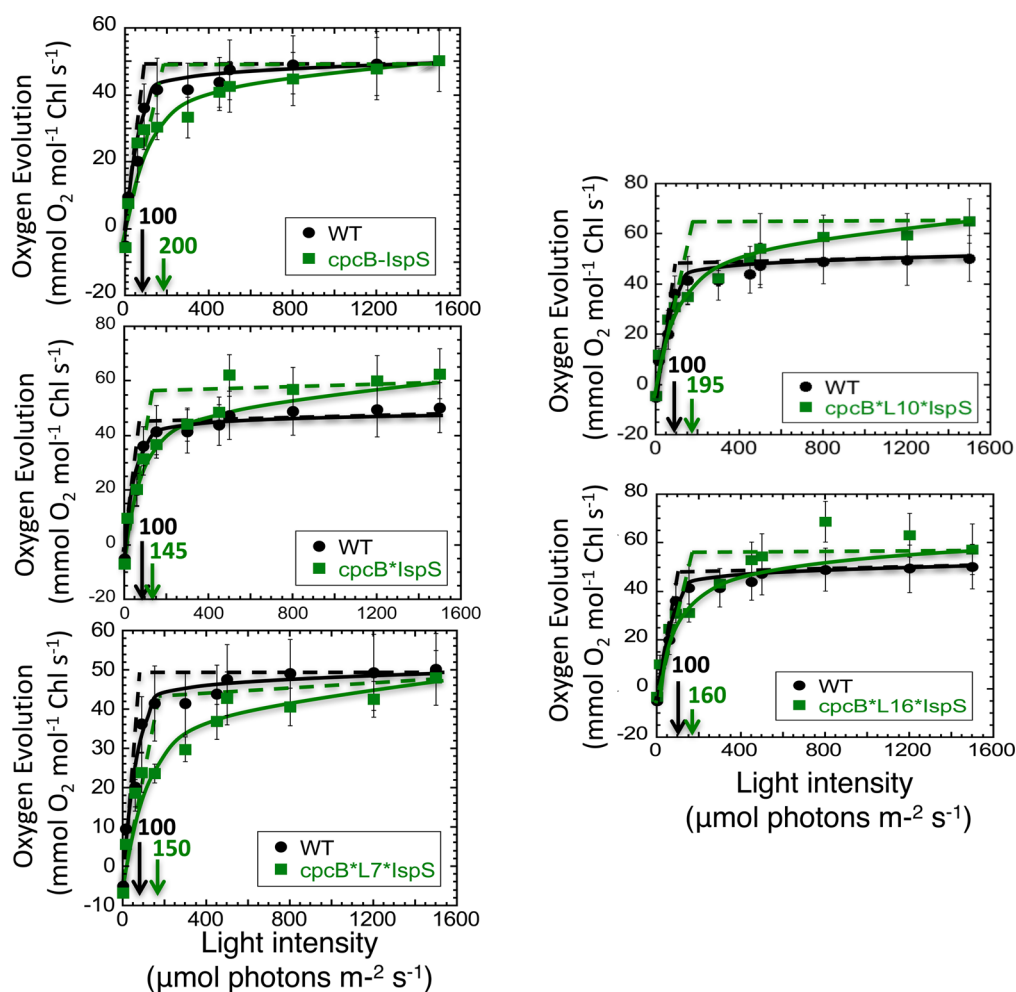


Figure 8. Light-saturation curves of photosynthesis. Oxygen evolution measurements of wild type, $cpcB-IspS$, $cpcB*IspS$ and $cpcB*L(7,10,16)*IspS$ strains were conducted with a Clark-type O_2 electrode. The rate of oxygen evolution was negative at zero light intensity and was determined to be in the range of 4 ± 1 mmol O_2 consumption mol^{-1} Chl s^{-1} in the $cpcB-IspS$, $cpcB*IspS$ and $cpcB*L(7,10,16)*IspS$ strains. Increase in the rate of oxygen evolution as a function of light intensity was steeper for the wild type than for the transformants resulting in dissimilar saturation intensities for the two groups. The light intensity for the saturation of photosynthesis was determined from the intersect of the initial linear increase in the rate of photosynthesis with the asymptotic light-saturated state–state rate (P_{max}). This analysis showed that photosynthesis in the wild type was saturated at about $100 \mu mol$ photons $m^{-2} s^{-1}$, whereas that of the transformants saturated at higher light intensities, ranging from 145 to $200 \mu mol$ photons $m^{-2} s^{-1}$.

whereas that of the transformants saturated at higher light intensities, ranging from 145 to 200 $\mu\text{mol photons m}^{-2} \text{s}^{-1}$ (Figure 8). A photosynthesis-saturation intensity in the 145 to 200 $\mu\text{mol photons m}^{-2} \text{s}^{-1}$ range was also noted for the *cpcB*L65*IspS* strain (not shown). The higher intensity for the saturation of photosynthesis in the transformants is attributed to their smaller light-harvesting antenna size, as they lack functional phycocyanin, have a truncated phycobilisome light-harvesting antenna¹⁹ and, therefore, a diminished absorption cross section for light-harvesting.

In spite of the different antenna configuration and light-saturation curves of photosynthesis in wild type and *IspS* transformants, all strains examined in this work showed about the same light-saturated rate of photosynthesis (P_{max}), equal to about $55 \pm 5 \text{ mmol O}_2 \text{ evolved mol}^{-1} \text{ Chl s}^{-1}$. These findings show that transformations performed to effect a change in the expression level of the *IspS* gene have altered the pigment characteristics and phycobilisome antenna size of *Synechocystis* but have not affected the basic cell photosynthetic capacity, metabolism, or fitness.

Rate of Cell Growth and Isoprene Accumulation. Cell growth and isoprene accumulation experiments were conducted using the gaseous-aqueous two-phase photobioreactor system designed by Bentley and Melis.⁶ Measurements of cell biomass accumulation were obtained either from the culture optical density at 730 nm ($\text{OD}_{730 \text{ nm}}$; Figure 9A) or from the dry cell weight (DCW; Figure 9B) of culture aliquots sampled as a function of growth time. All fusion strains (*cpcB*IspS*,

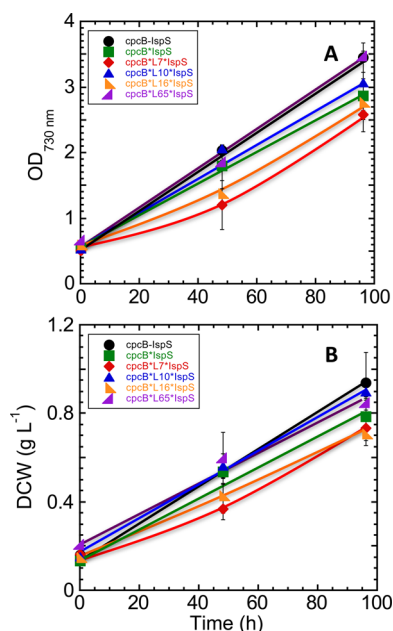


Figure 9. Biomass accumulation in *Synechocystis* liquid cultures. Liquid cultures of all strains were grown using the gaseous-aqueous two-phase bioreactor method, supplemented with 500 mL 100% CO_2 to fill the headspace, sealed, and stirred slowly under continuous illumination of 100 $\mu\text{mol photons m}^{-2} \text{s}^{-1}$ intensity. Biomass accumulation was measured every 48 h for 96 h total by (A) optical density of the liquid culture and (B) by dry cell weight. All *cpcB*IspS* fusion strains (*cpcB*IspS*, *cpcB*L(7,10,16,65)*IspS*) grew at a rate similar to that of the control (*cpcB-IspS*). Two of the fusion strains, *cpcB*L7*IspS* and *cpcB*L16*IspS* showed a slight lag in their initial growth (0–48 h) and then continued to grow at a rate comparable with that of the other strains.

*cpcB*L(7,10,16,65)*IspS*) grew at a rate similar to that of the control (*cpcB-IspS*) (Figure 9). Two of the fusion strains, *cpcB*L7*IspS* and *cpcB*L16*IspS* showed a slight lag in their initial growth (0–48 h) and then continued to grow with a rate comparable to that of the other strains (Figure 9). Rates of cell growth and biomass accumulation were estimated from the slope of the linear biomass increase (48–96 h). Under our experimental conditions, the average rate of biomass accumulation among all strains was about $6.9 \text{ mg dcw L}^{-1} \text{ h}^{-1}$ (Figure 9B). Rates of biomass accumulation for each of the individual strains examined in this work are reported in Table 2.

Isoprene accumulated in the reactor headspace concomitant with cell growth. Unlike the rate of biomass, rate of isoprene accumulation differed substantially between the different transformants (Figure 10A). All fusion strains produced more isoprene than the *cpcB-IspS* control. The latter generated about $1.7 \mu\text{g L}^{-1} \text{ h}^{-1}$, whereas the fusion strain without a linker (*cpcB*IspS*) produced about $5.8 \mu\text{g L}^{-1} \text{ h}^{-1}$. The strain with the 65 amino acids linker (*cpcB*L65*IspS*) generated isoprene at slightly greater yields ($7.6 \mu\text{g L}^{-1} \text{ h}^{-1}$). The *cpcB*L16*IspS* strain produced $10.3 \mu\text{g L}^{-1} \text{ h}^{-1}$, and the *cpcB*L10*IspS* produced $15.3 \mu\text{g L}^{-1} \text{ h}^{-1}$. The highest overall producer was the *cpcB*L7*IspS* strain, generating about $28.9 \mu\text{g L}^{-1} \text{ h}^{-1}$ (Table 2).

Isoprene-to-biomass (w:w) partition ratios provide a more pertinent measurement of the yield of the process. Such ratios are also shown in Table 2. Strain *cpcB*IspS* showed a 4.5-fold increase in the yield of isoprene, over what was measured with the *cpcB-IspS* nonfusion transformant. By the same token, strain *cpcB*L7*IspS* showed a 27-fold increase in the yield of isoprene, over what was measured with the *cpcB-IspS* nonfusion transformant. Intermediate gains were observed with the other linker constructs. For better visualization of the results, the isoprene-to-biomass (w:w) partition ratio was plotted for the various strains examined in this work (Figure 10B).

A relative measure of the specific activity, *i.e.*, efficacy of the different *IspS* fusion configurations to generate isoprene was offered from the isoprene-to-biomass ratio normalized for the relative quantity of the enzyme present in the different transformants (Figure 5). These estimates are shown in Table 2, column 5. It is seen that the nonfusion configuration of the *IspS* (*cpcB-IspS*) has the highest specific activity ($200 \mu\text{g Isp g}^{-1} \text{ Bms [Isp]}^{-1}$), whereas the fusion without linker (*cpcB*IspS*) has the lowest specific activity ($3.27 \mu\text{g Isp g}^{-1} \text{ Bms [Isp]}^{-1}$). L10, L16, and L7 transformants showed intermediate levels of *IspS* specific activity. These results are evidence that specific activity was compromised in all fusion transformants, possibly because of allosteric effects exerted by the leader *cpcB* fusion protein, albeit this inhibition was substantially modulated by the nature of the linker amino acids placed between the *cpcB* and *IspS* proteins. In terms of isoprene production, the results further showed a trade-off between specific activity and amount of transgenic enzyme accumulation. For example, the *cpcB*L7*IspS* strain showed only about 10% the isoprene synthase specific-activity of the unfused *cpcB-IspS* control but it accumulated a 254-fold greater amount of *IspS* enzyme. The latter more than countered the lower specific activity and contributed to making the *cpcB*L7*IspS* strain the best isoprene producing strain in this work.

The *cpcB*IspS* and the *cpcB*L7*IspS* transformants accumulated equivalent amounts of the transgenic fusion protein (Figure 4), but produced substantially different

Table 2. *Synechocystis* Liquid Cultures Were Cultivated in Gaseous–Aqueous Two-Phase Photobioreactors for 96 h upon Provision of 500 mL of 100% CO₂ To Fill the Reactor Headspace^a

strain	rate of biomass accumulation (mg L ⁻¹ h ⁻¹)	rate of isoprene accumulation (μg L ⁻¹ h ⁻¹)	isoprene to biomass ratio (mg g ⁻¹)	IspS specific activity (μg Isp g ⁻¹ Bms [IspS] ⁻¹)
cpcB-IspS	8.1 ± 0.32	1.7 ± 0.32	0.2 ± 0.05	200 ± 50.0
cpcB*IspS	6.8 ± 1.20	5.8 ± 0.62	0.9 ± 0.16	3.27 ± 0.60
cpcB*L65*IspS	6.7 ± 0.07	7.6 ± 0.62	1.1 ± 0.22	4.70 ± 0.94
cpcB*L16*IspS	5.8 ± 0.27	10.3 ± 1.28	1.6 ± 0.45	23.9 ± 7.00
cpcB*L10*IspS	8.3 ± 0.74	15.3 ± 2.18	1.8 ± 0.33	29.5 ± 5.41
cpcB*L7*IspS	5.4 ± 0.18	28.9 ± 1.06	5.4 ± 0.49	21.3 ± 1.93

^aContinuous illumination of 100 μmol photons m⁻² s⁻¹ and temperature of 25 °C were applied during cultivation. Rates of biomass (mg L⁻¹ h⁻¹), isoprene (μg L⁻¹ h⁻¹), and isoprene to biomass ratio (mg g⁻¹) were calculated for each strain. The IspS specific activity (μg Isp g⁻¹ Bms [IspS]⁻¹) was estimated from the isoprene to biomass ratio normalized to the relative IspS content in the respective biomass.

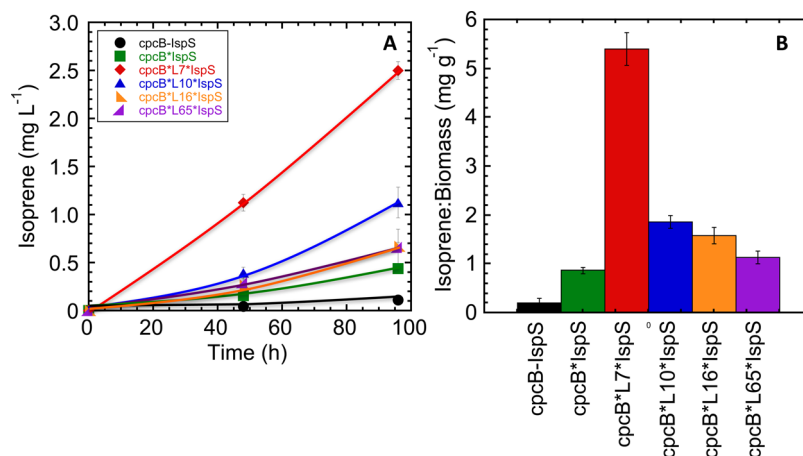


Figure 10. Isoprene accumulation in the reactor gaseous phase. Measurements were taken concurrently with those for biomass accumulation, every 48 h for a total of 96 h. Gas chromatography was employed to analyze 1 mL samples taken from the headspace using a gastight syringe. Isoprene quantification was based on a calibration of isoprene standard (Acros Organics, Fair Lawn, NJ, USA), as described (Chaves *et al.*²¹). Note the dissimilar rates of isoprene accumulation.

amounts of isoprene. These results suggested that the cpcB*L7*IspS fusion was substantially more active in catalysis than the cpcB*IspS counterpart. A question was asked as to whether fusion of the cpcB to the IspS in the cpcB*IspS construct impedes substrate access to the catalytic site, and whether the L7 linker changed the stereochemical and spatial relationship between the cpcB and IspS proteins, making the catalytic site of the isoprene synthase enzyme more easily accessible to the DMAPP substrate, thus leading to higher rates of isoprene synthesis? These two hypotheses, enzyme catalytic activity and stereochemistry of the fusion constructs, were investigated in greater detail.

Enzymatic Properties of cpcB*IspS, cpcB*L7*IspS, and cpcB*L16*IspS *In Vitro*. To determine the effect of the cpcB*IspS fusion, and that of the linker amino acids, on the isoprene synthase specific catalytic activity, *in vitro* assays were conducted on the enzymatic properties of the lowest (cpcB*IspS), intermediate (cpcB*L16*IspS), and highest (cpcB*L7*IspS) isoprene producers. Highly concentrated *Synechocystis* cell lysates of each of the strains were used as the catalyst for the *in vitro* reactions. Aliquots of each soluble cell lysate fraction were run on an SDS-PAGE gel to determine the concentration of the cpcB*IspS, cpcB*L16*IspS, and cpcB*L7*IspS enzymes relative to a bovine serum albumin (BSA) standard (Figure 11). For example, BSA samples were loaded at 0.2, 0.4, 0.6, 0.8, and 1.0 μg per lane to establish a calibration curve of the 66.5 kDa band density, measured by the Bio-Rad Image Lab software, as a function of protein amount

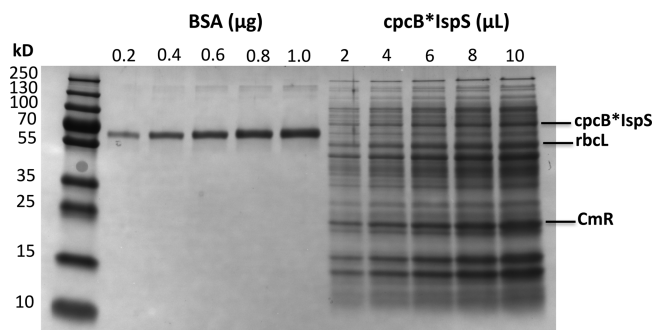


Figure 11. Calibration of protein content. Liquid cultures of *Synechocystis* containing the fusion isoprene synthase construct cpcB*IspS were grown in 5 L cultures, cells were concentrated, and lysed by French press. The soluble fraction of the cell lysate was then filtered and further concentrated using Amicon Ultra 15 50 kDa filters (Millipore, USA). Aliquots of the concentrated crude cell extracts were solubilized, proteins resolved in SDS-PAGE, and stained with Coomassie brilliant blue. Protein concentrations were determined based on the intensity of the cpcB*IspS fusion protein appearing at 85 kDa relative to a BSA standard. The Bio-Rad ChemiDoc imaging system was used to document the Coomassie-stained intensity of the bands and the Bio-Rad Image Lab software was employed to quantify the relative IspS protein levels from the different strains relative to that of BSA.

loaded (Figure 11, BSA). Similarly, cell lysates from the cpcB*IspS fusion strain were loaded at five different volumes

(2, 4, 6, 8, and 10 μL) in parallel with the BSA standard (Figure 11, cpcB*IspS). This SDS-PAGE analysis showed the cpcB*IspS fusion protein band migrating to about 84 kDa, while the rbcL and Cmr proteins were also visible, migrating to 58 and 24 kDa, respectively (Figure 11, cpcB*IspS). Such comparative protein calibration approach helped define the cell lysate volume that contained 12 μg of BSA-equivalent of the cpcB*L7*IspS fusion protein. The latter was used in the isoprene synthase enzymatic kinetic analysis undertaken in this work (see work below).

A similar comparative SDS-PAGE protein loading calibration approach was undertaken for the cell lysates from the cpcB*L7*IspS (Supporting Information, Figure S1) and cpcB*L16*IspS (Supporting Information, Figure S2) strains, which helped define the cell lysate volume that contained 12 μg of BSA-equivalent cpcB*L7*IspS and cpcB*L16*IspS proteins.

In vitro isoprene synthesis reactions were conducted in the presence of varying concentrations of DMAPP at 42 °C for 15 min.¹⁴ Volatile products collected in the headspace of the reaction vessel were subjected to gas chromatography analysis to quantify isoprene yields.²¹ Reaction mixtures without cell lysate were used as a control. These did not produce any isoprene. Lineweaver–Burk analysis of the enzymatic kinetics of isoprene production were calculated and plotted. An example of such analysis is given in Figure 12 for the cpcB*L7*IspS

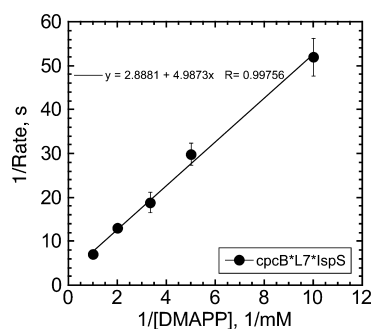


Figure 12. Lineweaver–Burk plot of the IspS enzymatic kinetic analyses. *In vitro* IspS enzymatic reactions of the cpcB*L7*IspS fusion protein were conducted in 100 μL mixtures containing 50 mM Bicine, pH 8.0, 30 mM NaCl, 50 mM MgCl_2 , 50 mM KCl, 5% glycerol, 1 mM DTT, 12 μg cpcB*LX*IspS, and varying concentrations of DMAPP. Reaction mixtures were incubated for 15 min at 42 °C, then 1 mL aliquots from the headspace were sampled for isoprene content by gas chromatography.

fusion protein. Addition of the L7 linker conferred isoprene synthase enzymatic properties with a $k_{\text{cat}} = 0.346 \text{ s}^{-1}$, $K_m = 1.73 \text{ mM}$, and $V_{\text{max}} = 0.250 \mu\text{mol (mg protein)}^{-1} \text{ min}^{-1}$ (Figure 12 and Table 3). The Lineweaver–Burk plot of the cpcB*IspS fusion protein (Supporting Information, Figure S3) showed a nearly flat line, indicating a slow enzymatic activity with minimal dependence on substrate (DMAPP) concentration, consistent with the slow *in vivo* IspS specific activity of this construct. Analysis of the results showed a $k_{\text{cat}} = 0.0159 \text{ s}^{-1}$, $K_m = 0.0145 \text{ mM}$, and $V_{\text{max}} = 0.0113 \mu\text{mol (mg protein)}^{-1} \text{ min}^{-1}$ (Supporting Information, Figure S3 and Table 3). Addition of the amino acids linker L16 in the cpcB*L16*IspS fusion protein enhanced the catalytic activity of the enzyme, relative to that of the cpcB*IspS, by about 2-fold, also consistent with the *in vivo* isoprene yields. The cpcB*L16*IspS enzyme displayed a $k_{\text{cat}} = 0.0318 \text{ s}^{-1}$, $K_m = 1.30 \text{ mM}$, and $V_{\text{max}} = 0.0225 \mu\text{mol (mg protein)}^{-1} \text{ min}^{-1}$ (Supporting Information, Figure S4 and

Table 3. *In Vitro* IspS Enzyme Kinetics Were Measured with Crude Protein Extracts from the Fusion Strains cpcB*IspS, cpcB*L16*IspS, and cpcB*L7*IspS^a

construct	k_{cat} (s^{-1})	K_m (mM)	V_{max} $\mu\text{mol (mg protein)}^{-1} \text{ min}^{-1}$
cpcB*IspS	0.016 ± 0.002	0.015 ± 0.002	0.011 ± 0.002
cpcB*L16*IspS	0.032 ± 0.006	1.30 ± 0.420	0.023 ± 0.005
cpcB*L7*IspS	0.350 ± 0.020	1.73 ± 0.225	0.250 ± 0.018

^aReactions were conducted in 100 μL mixtures containing 50 mM Bicine, pH 8.0, 30 mM NaCl, 50 mM MgCl_2 , 50 mM KCl, 5% glycerol, 1 mM DTT, 12 μg of BSA-equivalent cpcB*LX*IspS protein extract, and varying concentrations of DMAPP. Reactions were incubated for 15 min at 42 °C, then 1 mL aliquots of the headspace were sampled for isoprene content by gas chromatography. k_{cat} , K_m , and V_{max} were calculated from Lineweaver–Burk plots of the reaction parameters for each fusion enzyme.

Table 3). In sum, the cpcB*L7*IspS strain had the highest specific activity, 22-fold greater than that of the cpcB*IspS. A summary of the enzymatic properties of the cpcB*IspS, cpcB*L16*IspS, and cpcB*L7*IspS fusion enzymes is given in Table 3.

Modeling. To further address the question of whether fusion of the cpcB to the IspS impedes catalytic activity, and whether the linkers change the stereochemical and spatial relationship between the cpcB and IspS proteins, making the catalytic site of the isoprene synthase enzyme more easily accessible to the substrate, thus leading to higher rates of isoprene synthesis, protein folding modeling was undertaken. RaptorX software²² analysis of the cpcB*IspS fusion showed the cpcB protein with the N-terminus and the subsequent two short α -helices exposed (Figure 13A, blue arrow). In this cpcB*IspS fusion model, the IspS folded near and to the east side of the cpcB. The first nine amino acids of the IspS are shown facing the medium immediately after the last amino acid of the cpcB protein (Supporting Information Figure S6, white arrow). This configuration resulted in a slow catalytic activity and uncompetitive inhibition of the IspS (Tables 2 and 3).

In the subsequent RaptorX software analysis, an effort was made to orient the fusion construct structures with respect to the N-terminus coordinates of the cpcB protein, as this shown in Supporting Information Figure S6. In the cpcB*L7*IspS folding model (Figure 13B), the IspS is shown to have flipped by more than 180 deg to the west of the cpcB relative to the orientation shown in the folding model cpcB*IspS. Similarly, the cpcB*L10*IspS (Figure 13C) and the cpcB*L16*IspS (Figure 13D) showed the IspS rotated to the west of the cpcB. The cpcB*L65*IspS was rotated to an even greater degree (about 270 deg), with the IspS positioned to the south of the cpcB (Figure 13E). Each linker increased the distance between the two proteins, and caused a slightly different orientation of the IspS relative to the cpcB, both of which appear to contribute to the differing enzymatic activities. An amino acid alignment of several IspS enzymes from different plant species¹⁴ showed conserved regions among the isoprene synthases, especially so at the N-terminal domain comprising tandem arginine residues followed by an absolutely conserved tryptophan residue. This highly conserved RR(X)₃W terpene synthase motif (amino acid residues 17 through 28 from the N-terminus of the mature protein) was suggested to play a role in diphosphate walking and/or terpene cyclization reactions^{23,24} and is present in all terpene synthases. It appears that use of different amino acid spacers changed the relative orientation

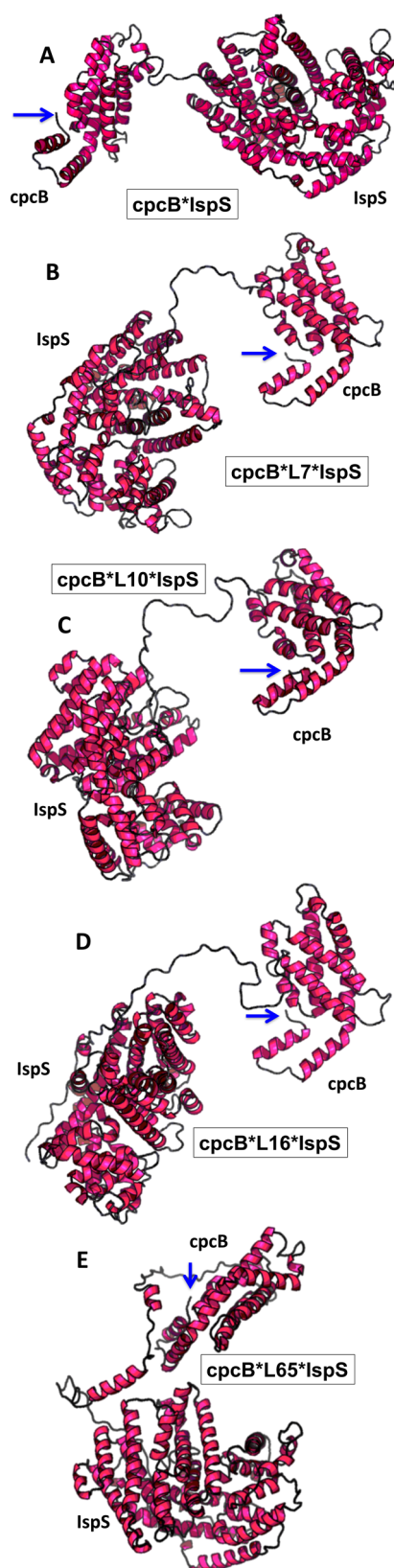


Figure 13. RaptorX software was employed to visualize possible folding patterns of the various cpcB and IspS fusion proteins. (A) *cpcB*IspS*, (B) *cpcB*L7*IspS*, (C) *cpcB*L10*IspS*, (D) *cpcB*L16*IspS*, (E) *cpcB*L65*IspS*. Protein models have been oriented with respect to the cpcB protein, with the N-terminus of the cpcB marked by a blue arrow. Note the substantially different orientation and distance of the IspS relative to the cpcB in the

Figure 13. continued

*cpcB*IspS* versus the *cpcB*L7*IspS*, *cpcB*L10*IspS*, *cpcB*L16*IspS*, and *cpcB*L65*IspS* constructs.

and distance of the cpcB relative to the N-terminal domain of the IspS, and it may thus impact the function of the IspS N-terminal domain RR(X)8W motif comprising the conserved tandem arginine and tryptophan residues, thereby affecting activity.

DISCUSSION

Isoprene synthase enzymes have been studied *in vitro* to characterize their kinetic properties. This includes the *Populus alba* (poplar) and *Pueraria montana* (kudzu) IspS proteins.^{13,14,25} Further, the IspS gene was codon optimized and applied for expression to *Synechocystis*,⁵ showing the feasibility of driving the cyanobacterial photosynthesis and metabolism toward the heterologous production of isoprene. However, terpene synthases have notoriously slow turnover kinetics, and the kudzu isoprene synthase proved to fit in the family with a $k_{cat} = 4.4 \text{ s}^{-1}$, and $K_m = 2.5 \text{ mM}$.¹⁴ The present study conducted enzymatic kinetic analyses of the cyanobacterial codon-optimized kudzu IspS, as previously used in this lab, but with the enzyme in different fusion configurations with the cpcB protein (the β -subunit of phycocyanin), as this fusion construct was highly expressed in transformant *Synechocystis*. Although a direct fusion of the IspS to the cpcB gene (*cpcB*IspS*) substantially enhanced (275-fold) the concentration of the IspS protein in the cells (Figure 4 and 5), the catalytic ability of the enzyme was compromised with a specific activity (functional efficiency) equal to only 1.64% of the unfused enzyme.

The direct fusion of the cpcB to the isoprene synthase resulted in very low catalytic activity for the IspS enzyme. Our initial hypothesis was that the cpcB is interfering with and blocking substrate entrance to the catalytic site at the N-terminal domain of the IspS. To mitigate this potential interference, amino acid linkers were designed to separate the two proteins based on the secondary structure of the linker. The “L7” linker contains two prolines, designed to alter the relative orientation of the cpcB protein relative to the N-terminus of the IspS. It was hypothesized that this was a good candidate to alleviate interference/blocking substrate entrance to the catalytic site at the N-terminal domain of the IspS. The “L10” linker contains five repeating segments of proline and alanine (PA)₅. The small size of the proline, the cyclic side chain, and the lack of an amide hydrogen may prevent interactions with other amino acids in the main protein domains, and cause a very restricted, or rigid linker structure.²⁰ The “L16” contains repeat segments of (EAAAK), forming a rigid and stable α helix linker. These rigid linkers were thought to be ideal candidates to separate in different ways the cpcB and the IspS, while preventing the cpcB from moving freely around the IspS and potentially blocking the IspS N-terminal catalytic domain. The “L65” linker repeated the first 65 amino acids of the isoprene synthase. In repeating this segment, which contains the N-terminal catalytic domain of the IspS, we sought to induce any unfavorable cpcB folding with the L65 linker, and prevent it from occurring with the main protein N-terminal catalytic domain.

The use of amino acid spacers mitigated the degree to which the enzymatic activity was inhibited by the direct cpcB fusion,

while retaining the high level of the fusion protein. For example, the best isoprene producer (*cpcB**L7**IspS*) resulted in a 254-fold increase in the concentration of the *IspS* protein in the cells and had a specific activity 10.65% of the unfused enzyme. Thus, the combined result of specific activity times enzyme concentration translated in superior yields, as evidenced by the productivity of the *cpcB**L7**IspS* strain, when compared to the unfused control (*cpcB*-*IspS*). Overall, the large increase in enzyme concentration outweighed the decrease in specific activity in terms of isoprene production, resulting in 27-fold gains in production compared to nonfused *IspS*. This compares favorably to recent independent attempts at improving the catalytic activity of an *IspS* enzyme through directed evolution, which resulted in modest improvements, *i.e.*, 1.6- to 1.8-fold increase in isoprene production yield.⁴ Together, these results show that concentration of the isoprene synthase enzyme and its specific activity are substantially important determinants of yield in the cyanobacterial isoprene production process.

The results further showed that linker length and the associated distance by which to separate the *cpcB* and *IspS* proteins is not an important variable in the activity of the *IspS*. For example, the short L7 linker resulted in the highest specific activity measured in this work, whereas the long linkers (L16 and L65) yielded mixed results. Thus, the work showed that linker length is not an important determinant in *cpcB**L**IspS* fusion protein activity but, rather, the relative folding of the two proteins with respect to one another is what defined *IspS* rate of catalysis.

Alleviating bottlenecks in the MEP isoprenoid biosynthetic pathway toward isoprene production included attempts to alleviate rate-limiting enzymatic steps, such as those defined by the DXS,^{26–29} DXR,^{27,30} and the IPP isomerase.^{9,10} As endogenous carbon partitioning to the MEP pathway is limited,⁵ coexpression of feeding pathways such as the Embden-Meyerhof pathway (EMP) and Entner-Doudoroff Pathway (EDP)(26) have resulted in enhanced isoprenoid production in *E. coli*. Cellular concentrations of the universal isoprenoid precursors (DMAPP and IPP) are also limiting, and use of acetyl-CoA as an additional primary substrate feedstock through an exogenous mevalonic acid pathway improved isoprenoid production in both *Synechocystis*⁶ and *E. coli*.^{14,31} Thus, the combination of improved global carbon flux to DMAPP with overexpression of the *IspS* fused to the *cpcB* is promising in efforts to generate even greater yields of isoprene.⁷

A goal of biotechnology today is to develop the ability of utilizing sunlight, CO₂, and water in order to renewably generate fuel and chemicals as efficiently as possible. Cyanobacteria offer a unique opportunity to develop such technologies, with the microorganism acting as a single-cell factory, capturing carbon dioxide and converting it into useful products. This work contributed to the identification of a barrier in the renewable generation of isoprene through photosynthesis in cyanobacteria and further provided evidence of ways by which to alleviate some of the associated level-of-expression problems.

MATERIALS AND METHODS

Strains and Culturing Conditions. *Synechocystis* sp. PCC 6803 was employed as the experimental strain and is referred to as the wild type (WT). All strains employed in this work were maintained on 1% agar-BG11 media supplemented with 10 mM TES-NaOH pH 8.2, and 0.3% Na-thiosulfate. Chlor-

amphenicol (30 μg/mL), was added to the agar plates and used to maintain transformants. Liquid cultures were grown in BG11 media buffered with 25 mM NaH₂PO₄ (pH 7.5) at 28 °C, under continuous aeration and gradually increasing illumination. Cultures inoculated from a plate started in the lowest illumination at 30 μmol photons m⁻² s⁻¹ until an OD_{730 nm} = 0.3 was reached. Illumination was then increased to 50 μmol photons m⁻² s⁻¹ until an OD_{730 nm} = 0.65–0.75 was reached. Illumination was then increased to 100 μmol photons m⁻² s⁻¹ until the culture reached a density great enough to support dilution in 700 mL to an OD_{730 nm} = 0.65. The latter was subjected to 100% CO₂-loading in the sealed Bentley and Melis⁶ gaseous-aqueous two-phase bioreactor for biomass and isoprene quantification.

IspS-Containing Constructs. Transformations were performed as previously established.¹⁹ DNA constructs were designed to insert the isoprene synthase (*IspS*) gene in the *cpc* operon locus. In the control strain (*cpcB*-*IspS*), the isoprene synthase gene along with the chloramphenicol resistance cassette were inserted between the *cpcB* and *cpcA* coding regions with a ribosome-binding site placed in front of each. In alternative configurations engineered for isoprene synthase overexpression, the isoprene synthase was designed as a fusion with the *cpcB* gene (*cpcB***IspS*), either with or different nucleotide spacers between the two genes, which translated into amino acid spacers in the fusion protein. Four different amino acid spacers were designed as links between the *cpcB* and *IspS* proteins consisting of the following:

- i. L7: A single proline followed by the final 6 amino acids of the putative *IspS* transit peptide, PMPWRVI (*cpcB**L7**IspS*),
- ii. L10: A total of five alternating proline-alanine pairs PAPAPAPAPA (*cpcB**L10**IspS*),
- iii. L16: A combination of 16 amino acids comprising glutamic acid (E), alanine (A), lysine (K), EAAAKEAAAKEAAKA (*cpcB**L16**IspS*), and
- iv. L65: Comprising the 60 N-terminus amino acids of the isoprene synthase itself followed by 5 amino acids of the *IspS* transit peptide, CPWRVICATSSQFTQI-TEHNSRRSANYQPNLWNFEFLQSLNDLKVCKLE- EKATKLEEEVRPWRVI (*cpcB**L65**IspS*).

Pigment Analysis. Chlorophyll *a* and carotenoids were extracted from the cells in 100% methanol. The absorbance of the methanol extract was measured at 665 and 470 nm, corrected for any nonspecific absorbance at 710 nm. For this purpose, absorbance spectra of cell extracts were scanned spectrophotometrically from 400 to 750 nm with a Shimadzu UV-1800 UV-visible spectrophotometer. Readings of the absorbance at the above wavelengths were taken from the spectra. Pigment concentrations were calculated from the absorbance at these wavelengths according to equations given by Lichtenthaler.³² Cell lysates were collected by French press disruption as described below. Broken cell suspensions were then centrifuged at 2250g for 3 min to pellet cell debris and glycogen grains.

Protein Analysis. Cells were grown in 300 mL liquid cultures to an OD₇₃₀ of 2.5, pelleted by centrifugation, and resuspended in 5–10 mL of 50 mM Tris-HCl (pH 8). Protease inhibitor (1 mM PMSF) was added to samples before lysing of the cells by French press (2 × 1500 psi). Disrupted cell suspensions were centrifuged at 2250g for 3 min to pellet cell debris and glycogen grains. An aliquot of the supernatant was

used for pigment concentration determination, as described above. The supernatant was supplemented with an equal volume of solubilization solution, comprising 250 mM Tris-HCl, pH 6.8, 7% w/v SDS, 20% w/v glycerol, 2 M urea, and a few grains of bromophenol blue. Samples were solubilized upon incubation at room temperature for 1–2 h. At the end of the solubilization incubation, samples were supplemented with 5% β -mercaptoethanol. The solubilized total cellular proteins were subjected to SDS-PAGE and Western blot analysis. SDS-PAGE-resolved proteins were either stained with Coomassie brilliant blue or transferred to a nitrocellulose membrane for immunodetection using rabbit immune serum containing specific polyclonal antibodies against the IspS protein.⁵

Isoprene and Biomass Accumulation. Liquid cultures for biomass accumulation and isoprene production were grown photoautotrophically in the absence of antibiotics. Glass bottle bioreactors (1 L volume) were designed in this lab specifically for quantitative biomass and isoprene production measurements.⁶ The 1-L bioreactors were loaded with ~700 mL liquid BG11 growth medium containing 25 mM NaH_2PO_4 (pH 7.5), and then inoculated with *Synechocystis* starter cultures to an $\text{OD}_{730\text{ nm}} = 0.65$. Unless otherwise indicated, the bioreactors were further loaded with inorganic carbon, delivered to the liquid culture by slowly bubbling 500 mL of 100% CO_2 gas through the bottom of the liquid culture to fill the reactor headspace. Bioreactors were then sealed and cultures were stirred slowly and continuously at 28 °C under constant illumination at 100 $\mu\text{mol photons m}^{-2} \text{s}^{-1}$.

Isoprene accumulation in the headspace of the reactor was determined by gas chromatography (Shimadzu 8A GC-FID) analysis of 1 mL gaseous samples from the bioreactor headspace. Isoprene quantification was determined based on a calibration of isoprene standard (Acros Organics, Fair Lawn, NJ, USA), as described.²¹ Biomass accumulation in the liquid phase of the reactor was determined upon collection of 50 mL aliquots, followed by centrifugation, rinsing of the pellet with deionized water, and cell resuspension in 2 mL of deionized water. The latter were transferred onto aluminum trays, dried for 6 h at 90 °C, and weighed to determine the dry cell weight (dcw). Cell growth was also determined spectrophotometrically by measuring the optical density of live cell cultures at 730 nm with a Shimadzu UV-1800 UV–visible spectrophotometer.

Photosynthetic Activity. Oxygen evolution of the cells was measured with a Clark-type oxygen electrode (Oxygraph Plus System, Hansatech Instruments Ltd., United Kingdom) at 23 °C illuminated with a high intensity 100 W tungsten-halogen light source. Cell suspensions were loaded into the oxygen electrode chamber at a concentration of 0.6 μM chlorophyll in 2 mL samples. Sodium bicarbonate (20 μL of 0.5 M solution, pH 7.4) was added to the samples just before measuring to prevent carbon limitation during photosynthesis. After determining the rate of dark respiration, the cells were illuminated with gradually increasing light intensities. Oxygen evolution was recorded for 2–5 min at each light intensity allowing linear progression of the slope.

In Vitro Assay Enzymatic Activity. Liquid cultures of *Synechocystis* strains containing the fusion isoprene synthase constructs (*cpcB**IspS**, *cpcB*L16**IspS**, *cpcB*L7**IspS**) were grown in 5 L cultures to an $\text{OD} = 3.5$, pelleted by centrifugation at 4000g for 15 min, resuspended in buffer (50 mM bicine, pH 8.0, 30 mM NaCl, 50 mM MgCl_2 , 50 mM KCl, 5% glycerol, 1 mM DTT), and lysed by French press (2×1500 psi). Disrupted cell suspensions were centrifuged at 2250g for 3

min to pellet cell debris and glycogen grains. The membranes of crude cell lysates were separated by ultracentrifugation at 143 000g for 60 min. The soluble fraction of the cell lysate was then filtered and concentrated using Amicon Ultra 15 50 kDa filters (Millipore, USA). Aliquots of the concentrated crude cell extracts were then run on an SDS PAGE gel and stained with Coomassie brilliant blue. Protein concentrations were determined based on the intensity of the *cpcB**IspS** fusion protein appearing as a band at 85 kDa relative to a BSA standard. The Bio-Rad ChemiDoc imaging system was used to photograph the Western blot and the Bio-Rad Image Lab software was utilized to quantify the relative *IspS* protein levels between the different strains based on band intensity.

In vitro reactions were conducted in 100 μL mixtures containing 50 mM Bicine, pH 8.0, 30 mM NaCl, 50 mM MgCl_2 , 50 mM KCl, 5% glycerol, 1 mM DTT, 12 μg *cpcB*LX**IspS**, and varying concentrations of DMAPP, as described.¹⁴ Reactions were incubated for 15 min at 42 °C, then 1 mL aliquots of the headspace were sampled for isoprene content by gas chromatography, as described above.

■ ASSOCIATED CONTENT

📄 Supporting Information

The Supporting Information is available free of charge on the ACS Publications website at DOI: 10.1021/acssynbio.7b00214.

DNA constructs employed in this work (*cpcB**IspS**, *cpcB*L7**IspS**, *cpcB*L10**IspS**, *cpcB*L16**IspS** and *cpcB*L65**IspS**); Figures S1–S10 (PDF)

■ AUTHOR INFORMATION

Corresponding Author

*Tel: 510-642-8166. Fax: 510-642-4995. E-mail: melis@berkeley.edu.

ORCID

Anastasios Melis: 0000-0003-2581-4177

Author Contributions

JEC, PRR, HK and AM designed the project. JEC and PRR conducted the experimental work. JEC and AM wrote the manuscript.

Notes

The authors declare the following competing financial interest(s): Some of the authors are inventors of intellectual property in the area of the publication. All co-authors reviewed the manuscript.

■ ACKNOWLEDGMENTS

The work was conducted in partial satisfaction of the requirements for the degree of Doctor of Philosophy by JEC, supported by a graduate student fellowship from the NSF Sage IGERT program. PRR was supported by a postdoctoral fellowship from the Ramón Areces Foundation.

■ ABBREVIATIONS

Bms, Biomass; CmR, Chloramphenicol resistance; cpc, Operon encoding the phycocyanin subunits and associated linker polypeptides; *cpcB*, First gene in the *cpc* operon encoding the β -phycocyanin subunit; *cpcB**IspS**, Isoprene synthase fusion to the *cpcB* gene; *cpcB*L7**IspS**, *cpcB*L10**IspS**, *cpcB*L16**IspS**, *cpcB*L65**IspS**, Isoprene synthase fusion to the *cpcB* gene with a spacer comprising 7, 10, 16, and 65 amino acids, respectively; dcw, Dry cell weight; DMAPP, Dimethyl-

lallyl-diphosphate; IPP, Isopentenyl diphosphate; Isp, Isoprene; IspS, Isoprene synthase; MEP, 2-C-Methyl-D-erythritol 4-phosphate; WT, Wild type

REFERENCES

- (1) Oliver, J. W., Machado, I. M., Yoneda, H., and Atsumi, S. (2014) Combinatorial optimization of cyanobacterial 2, 3-butanediol production. *Metab. Eng.* 22, 76–82.
- (2) Zhou, J., Zhang, H., Meng, H., et al. (2015) Discovery of a super-strong promoter enables efficient production of heterologous proteins in cyanobacteria. *Sci. Rep.* 4, 4500.
- (3) Kim, J.-H., Wang, C. L., Jang, H.-J., et al. (2016) Isoprene production by *Escherichia coli* through the exogenous mevalonate pathway with reduced formation of fermentation byproducts. *Microb. Cell Fact.* 15.1, 214.
- (4) Wang, F., Lv, X., Xie, W., Zhou, P., Zhu, Y., Yao, Z., Yang, C., Yang, X., Ye, L., and Yu, H. (2017) Combining Gal4p-mediated expression enhancement and directed evolution of isoprene synthase to improve isoprene production in *Saccharomyces cerevisiae*. *Metab. Eng.* 39, 257–66.
- (5) Lindberg, P., Park, S., and Melis, A. (2010) Engineering a platform for photosynthetic isoprene production in cyanobacteria, using *Synechocystis* as the model organism. *Metab. Eng.* 12, 70–79.
- (6) Bentley, F. K., and Melis, A. (2012) Diffusion-based process for carbon dioxide uptake and isoprene emission in gaseous/aqueous two-phase photobioreactors by photosynthetic microorganisms. *Biotechnol. Bioeng.* 109, 100–109.
- (7) Bentley, F. K., Zurbriggen, A., and Melis, A. (2014) Heterologous expression of the mevalonic acid pathway in cyanobacteria enhances endogenous carbon partitioning to isoprene. *Mol. Plant* 7 (1), 71–86.
- (8) Aremu, O., Borchert, C., Bastian, J. A., Knutson, A., Budzynski, C., Cai, J. Y., Chen, X., Guo, H., Lu, P., Venkataramanan, S. S., and Sethi, A. K. (2015) Inactivation of competing pathways and increased gene copies for enhanced isoprene production in *Synechococcus* sp. PCC 7002 Cyanobacteria, Thesis, University of Wisconsin.
- (9) Chaves, J. E., Romero, P., Kirst, H., and Melis, A. (2016) Role of isopentenyl-diphosphate isomerase in heterologous cyanobacterial (*Synechocystis*) isoprene production. *Photosynth. Res.* 130, 517–527.
- (10) Gao, X., Gao, F., Liu, D., Zhang, H., Nie, X., and Yang, C. (2016) Engineering the methylerythritol phosphate pathway in cyanobacteria for photosynthetic isoprene production from CO₂. *Energy Environ. Sci.* 9 (4), 1400–1411.
- (11) Pade, N., Erdmann, S., Enke, H., Dethloff, F., Dühring, U., Georg, J., Wambutt, J., Kopka, J., Hess, W. R., Zimmermann, R., and Kramer, D. (2016) Insights into isoprene production using the cyanobacterium *Synechocystis* sp. PCC 6803. *Biotechnol. Biofuels* 9 (1), 89.
- (12) Melis, A. (2013) Carbon partitioning in photosynthesis. *Curr. Opin. Chem. Biol.* 17, 453–456.
- (13) Sasaki, K., Ohara, K., and Yazaki, K. (2005) Gene expression and characterization of isoprene synthase from *Populus alba*. *FEBS Lett.* 579, 2514–2518.
- (14) Zurbriggen, A., Kirst, H., and Melis, A. (2012) Isoprene production via the mevalonic acid pathway in *Escherichia coli* (bacteria). *BioEnergy Res.* 5 (4), 814–828.
- (15) McNevin, D., von Caemmerer, S., and Farquhar, G. (2006) Determining RuBisCO activation kinetics and other rate and equilibrium constants by simultaneous multiple non-linear regression of a kinetic model. *J. Exp. Bot.* 57, 3883–3900.
- (16) Formighieri, C., and Melis, A. (2014) Regulation of β -phellandrene synthase gene expression, recombinant protein accumulation, and monoterpene hydrocarbons production in *Synechocystis* transformants. *Planta* 240, 309–324.
- (17) Formighieri, C., and Melis, A. (2015) A phycocyanin β -phellandrene synthase fusion enhances recombinant protein expression and β -phellandrene (monoterpene) hydrocarbons production in *Synechocystis* (cyanobacteria). *Metab. Eng.* 32, 116–124.
- (18) Formighieri, C., and Melis, A. (2016) Sustainable heterologous production of terpene hydrocarbons in cyanobacteria. *Photosynth. Res.* 130, 123–135.
- (19) Kirst, H., Formighieri, C., and Melis, A. (2014) Maximizing photosynthetic efficiency and culture productivity in cyanobacteria upon minimizing the phycobilisome light-harvesting antenna size. *Biochim. Biophys. Acta, Bioenerg.* 1837 (10), 1653–1664.
- (20) Chen, X., Zaro, J. L., and Shen, W. C. (2013) Fusion protein linkers: property, design and functionality. *Adv. Drug Delivery Rev.* 65 (10), 1357–1369.
- (21) Chaves, J. E., Kirst, H., and Melis, A. (2015) Isoprene production in *Synechocystis* under alkaline and saline growth conditions. *J. Appl. Phycol.* 27, 1089–1097.
- (22) Källberg, M., Wang, H., Wang, S., Peng, J., Wang, Z., Lu, H., and Xu, J. (2012) Template-based protein structure modeling using the RaptorX web server. *Nat. Protoc.* 7 (8), 1511–22.
- (23) Cunningham, F. X., Jr., Sun, Z., Chamovitz, D., Hirschberg, J., and Gantt, E. (1994) Molecular structure and enzymatic function of lycopene cyclase from the cyanobacterium *Synechococcus* sp strain PCC7942. *Plant Cell* 6 (8), 1107–1121.
- (24) Williams, D. C., McGarvey, D. J., Katahira, E. J., and Croteau, R. (1998) Truncation of limonene synthase preprotein provides a fully active 'pseudomature' form of this monoterpene cyclase and reveals the function of the amino-terminal arginine pair. *Biochemistry* 37 (35), 12213–12220.
- (25) Sharkey, T. D., Yeh, S., Wiberley, A. E., Falbel, T. G., Gong, D., and Fernandez, D. E. (2005) Evolution of the isoprene biosynthetic pathway in kudzu. *Plant Physiol.* 137 (2), 700–712.
- (26) Liu, H., Sun, Y., Ramos, K. R., Nisola, G. M., Valdehuesa, K. N., Lee, W. K., Park, S. J., and Chung, W. J. (2013) Combination of Entner-Doudoroff pathway with MEP increases isoprene production in engineered *Escherichia coli*. *PLoS One* 8 (12), e83290.
- (27) Lv, X., Xu, H., and Yu, H. (2013) Significantly enhanced production of isoprene by ordered coexpression of genes *dxs*, *dxr*, and *idi* in *Escherichia coli*. *Appl. Microbiol. Biotechnol.* 97 (6), 2357–2365.
- (28) Ramos, K. R., Valdehuesa, K. N., Liu, H., Nisola, G. M., Lee, W. K., and Chung, W. J. (2014) Combining De Ley–Doudoroff and methylerythritol phosphate pathways for enhanced isoprene biosynthesis from d-galactose. *Bioprocess Biosyst. Eng.* 37 (12), 2505–2513.
- (29) Xue, J., and Ahring, B. K. (2011) Enhancing isoprene production by genetic modification of the 1-deoxy-d-xylulose-5-phosphate pathway in *Bacillus subtilis*. *Appl. Environ. Microbiol.* 77 (7), 2399–2405.
- (30) Zhao, Y., Yang, J., Qin, B., Li, Y., Sun, Y., Su, S., and Xian, M. (2011) Biosynthesis of isoprene in *Escherichia coli* via methylerythritol phosphate (MEP) pathway. *Appl. Microbiol. Biotechnol.* 90 (6), 1915.
- (31) Yang, J., Xian, M., Su, S., Zhao, G., Nie, Q., Jiang, X., Zheng, Y., and Liu, W. (2012) Enhancing production of bio-isoprene using hybrid MVA pathway and isoprene synthase in *E. coli*. *PLoS One* 7 (4), e33509.
- (32) Lichtenthaler, H. K. (1987) Chlorophylls and carotenoids: pigments of photosynthetic biomembranes. *Methods Enzymol.* 148, 350–382.